Electronic Supplementary Material (ESI) for Sustainable Energy & Fuels.
This journal is © The Royal Society of Chemistry 2020

Metal Oxide Supported Ni-Impregnated Bifunctional Catalysts for Controlling Char Formation and Maximizing Energy Recovery during Catalytic Hydrothermal Liquefaction of Food Waste

Feng Cheng, Geoffrey A. Tompsett, Daniela Valeska Fraga Alvarez, Carla I. Romo, Amy M. McKenna, Sydney F. Niles, Robert K. Nelson, Christopher M. Reddy, Sergio Granados-Fócil, Alex D. Paulsen, Ruihan Zhang and Michael T. Timko

Supplemental Materials: Additional Tables and Figures.

Method of Food Waste Particle Size Measurement

The food waste slurry was dried in an oven at 60 °C for 48 hours and ground into fine particles prior to particle size measurement. The particle sizes present in the dried food waste were quantitatively determined using a microscope (Xplora, Horiba Scientific, Piscataway, NJ, USA). More than 100 particles were randomly selected and measured using the calibrated microscope, and the particle size distribution was reconstructed from this analysis.

GC-MS Method

The GC-MS consisted of a GC-2010 Plus gas chromatograph, a QP2010 SE mass spectrometer, and an AOC-20i autoinjector (Shimadzu Co., Kyoto, Japan). Products were separated on a SHRXI-5MS column (30 m × 0.25 mm ID × 0.5 μm film thickness) (Restek Co., Bellefonte, PA). The injection temperature was 290 °C and the ion source was held at 260 °C. The injection volume was 3 μL at a split ratio of 25:1. The helium carrier gas flow rate was set to 3.0 mL min^{-1}. The temperature program consisted of an initial set point of 30 °C, which was held for 4 min, followed by heating at 3 °C min^{-1} to 290 °C, and holding at the final temperature for 5 min. The mass spectrometer was operated in full-scan mode from 35–500 at unit resolution. Chromatograms were evaluated using the GCsolution Station (Shimadzu Co., Kyoto, Japan) and compared with the NIST Mass Spectral Database (NIST11). Top 30 the greatest peaks were tentatively discernible in the biocrude chromatograms, which could then be categorized based on chemical structure.

GC×GC-FID Method

GC×GC-FID chromatographic analyses were performed on a LECO GC×GC instrument consisting of an Agilent 7890A GC configured with a split/splitless auto-injector (7683B series) and a dual stage cryogenic modulator (LECO, Saint Joseph, Michigan). Samples were injected in splitless mode. The carrier gas was hydrogen at a constant flow rate of 1 mL min^{-1}. The cold jet gas was dry N_2 chilled with liquid N_2. The hot jet temperature offset was 15 °C above the temperature of the main GC oven and the inlet temperature was isothermal at 310 °C. Two capillary GC columns were utilized in this GC×GC experiment. The first-dimension column was a Restek Rxi-1ms, (60-m length, 0.25 mm I.D., 0.25 μm df) and second-dimension separations were performed on a 50% phenyl polysilphenylene-siloxane column (SGE BPX50, 1.2-m length, 0.10 mm I.D., 0.1 μm df). The temperature program of the main oven was held isothermal at 65 °C (12.5 min) and was then ramped from 50 to 340 °C at 1.25 °C min^{-1}. The second-dimension oven was isothermal at 70 °C (12.5 min) and then ramped from 70 to 345 °C at 1.25 °C min^{-1}. The hot jet pulse width was 1.00 seconds, while the modulation period between stages was 6.50 seconds and a 2.50 seconds cooling period. FID data was sampled at an acquisition rate of 100 data points per second.

GC×GC-HRT Method

GC×GC-HRT chromatographic analysis was performed on a LECO Pegasus GC×GC-HRT 4D system consisting of an Agilent 7890B GC configured with a LECO LPAL3 split/splitless auto-injector system and a dual stage cryogenic modulator (LECO, Saint Joseph, Michigan).[1] Samples were injected in splitless mode. The cold jet gas was dry N_2 chilled with liquid N_2. The hot jet temperature offset was 15 °C above the temperature of the main GC oven and the inlet temperature was isothermal at 310 °C. Two capillary GC columns were utilized in this GC×GC experiment. The first-

dimension column was an SGE BPX-50, (60-m length, 0.25 mm I.D., 0.25 μm df) and second-dimension separations were performed on an SGE BPX-50 (2-m length, 0.25 mm I.D., 0.25 μm df). The temperature program of the main oven was held isothermal at 80 °C (12.5 min) and was then ramped from 80 to 330 °C at 1.25 °C min^{-1}. The hot jet pulse width was 2 seconds with a modulation period of 8 seconds. The second-dimension oven was held isothermal at 85 °C (12.5 min) and was then ramped from 85 to 335 °C at 1.25 °C min^{-1}. The carrier gas was helium at a flow rate of 1 mL min^{-1}. Mass resolution was +/- 0.0005 amu. HR-TOF data was sampled at an acquisition rate of 200 spectra per second (actual data collection rate was 187.5 spectra per second) in the mass range of 40 to 700 amu. The ionization method was EI with an Electron Energy of -70 Volts and the Extraction Frequency was 1.5 kHz.

Sample preparation for 9.4 T APPI FT-ICR MS

All solvents were HPLC grade (Sigma-Aldrich Chemical Co., St. Louis, MO) and SPE extracts were dissolved in HPLC-grade tetrahydrofuran to yield a stock solution at 1 mg/mL, and further diluted to 250 μg/mL in toluene prior to analysis by positive ion atmospheric pressure photoionization (APPI).

Instrumentation for 9.4 T APPI FT-ICR MS

FT-ICR Mass Spectrometry and Data Analysis. Ions were generated at atmospheric pressure via an APPI source (Ion Max APPI source, Thermo-Fisher Scientific Inc., San Jose, CA, U.S.A.).[2] Samples extracts were analyzed with a custom-built FT-ICR mass spectrometer equipped with a 9.4 T superconducting solenoid magnet.[3] Ions were initially accumulated in an external multipole ion guide (1–5 ms) and released *m/z*-dependently by decrease of an auxiliary radio frequency potential between the multipole rods and the end-cap electrode.[4] Ions were excited to *m/z*-dependent radius to maximize the dynamic range and number of observed mass spectral peaks (32-64%),[5]

and excitation and detection were performed on the same pair of electrodes.[6] The dynamically harmonized ICR cell in the 9.4 T FT-ICR is operated with 6 V trapping potential.[3, 7] Time-domain transients of 7.2 seconds were acquired with the Predator data station, with 100 time-domain acquisitions averaged for all experiments.[8] Mass spectra were internally calibrated with five high-abundance homologous series that span the sample molecular weight distribution based on the "walking" calibration method.[9] Experimentally measured masses were converted from the International Union of Pure and Applied Chemistry (IUPAC) mass scale to the Kendrick mass scale[10] for rapid identification of homologous series for each heteroatom class (i.e., species with the same $C_cH_hN_nO_oS_s$ content, differing only be degree of alkylation).[11] For each elemental composition, $C_cH_hN_nO_oS_s$, the heteroatom class, type (double bond equivalents, DBE = number of rings plus double bonds to carbon, DBE = $C - h/2 + n/2 + 1$)[12] and carbon number, c, were tabulated for subsequent generation of heteroatom class relative abundance distributions and graphical relative-abundance weighted images and van Krevelen diagrams. Peaks with signal magnitude greater than 6 times the baseline root-mean-square (rms) noise at *m/z* 500 were exported to peak lists, and molecular formula assignments and data visualization were performed with PetroOrg © software.[13] Molecular formula assignments with an error >0.5 parts-per-million were discarded, and only chemical classes with a combined relative abundance of ≥0.15% of the total were considered.

Operation Procedure for Proton Nuclear Magnetic Resonance (^{1}H NMR) Spectroscopy

^{1}H-NMR spectra for the biocrude oils were acquired using a 400MHz Varian Mercury Plus NMR spectrometer. The bio-crude oil samples were prepared by dissolving ~10

mg in 500 µl of deuterated chloroform ($CDCl_3$) (Cambridge Isotope Laboratories, D 99.8%) containing 0.03 % (v/v) tetramethylsilane (TMS).

Total Acid Number Measurement

Total acid number (TAN) was measured by dissolving 10 mg of biocrude in 100 mL of absolute ethanol in a 250 mL beaker, forming a yellowish solution. Phenolphthalein (12–20 drops, 2 wt% ethanol) was added to the solution, which was then titrated with potassium hydroxide (0.02 M in ethanol) until the color started to turn pink. The titrant was standardized with potassium hydrogen phthalate.

Table S1. The estimated values of Ni particle size from the Ni-based catalysts.

Catalyst	**Ni particle size (Å)**	
	Fresh	**Used after HTL**
Ni/CeO_2	258	219
Ni/ZrO_2	253	175
$Ni/CeZrO_x$	259	215

Table S2. The elemental composition, higher heating value (HHV), and energy recovery (ER) of bio-crude oil and hydrochar, carbon yields of products, and gas composition from HTL (no H_2) of 15 wt% food waste under 300 °C for 60 min.

HTL (no H_2) Bio-crude Oil (wt%)					
C	**H**	**N**	**O[a]**	**HHV (MJ/kg)**	**ER (%)**
69.3 ± 0.9	8.8 ± 0.5	4.6 ± 1.1	17.4 ± 1.5	34.1 ± 2.7	27.1
Carbon Yields of HTL (no H_2) Products (wt%)					
Bio-crude Oil	**Aqueous**	**Solid**	**Gas**	**Loss[a]**	
23.8 ± 7.4	16.3 ± 3.1	41.4 ± 26.1	11.5 ± 2.7	6.8	
HTL (no H_2) Char (wt%)					

C	H	N	O[a]	HHV (MJ/kg)	ER (%)
69.7 ± 3.2	5.5 ± 0.2	5.1 ± 0.1	19.7 ± 3.2	29.0 ± 4.5	39.3

Composition of Gas Product (no H_2) (wt%)				
H_2	CO	CH_4	CO_2	C_2H_4
2.7	74.7	0	22.1	0.5

[a] By difference.

Table S3. Total acid number of bio-crude oil obtained using different catalysts.

	Thermal (H_2)	CeO_2	ZrO_2	$CeZrO_x$	Ni/CeO_2	Ni/ZrO_2	$Ni/CeZrO_x$
TAN[a] (mg KOH g^{-1} Bio-crude oil)	119±17	222±6	164±11	84±2	355±3	14±2	212±19
TOC[b] (g L^{-1}) in Aqueous Phase	13.0	14.1	17.3	15.2	21.1	21.0	26.9

[a] TAN: Total Acid Number. [b] TOC: Total Organic Content. Ranges represent the standard deviation of either two or three repeated tests.

Table S4. The elemental composition and higher heating value (HHV) of char.

Solids	C (wt.%)	H (wt.%)	N (wt.%)	O (wt.%)[a]	H/C Ratio	O/C Ratio	N/C Ratio	HHV (MJ kg^{-1})[b]
Food Waste	47.2	6.7	4.6	41.5	1.70	0.66	0.08	24.6
HTL(H_2)	72.1 ± 1.6	5.8 ± 0.2	5.6 ± 0.4	16.5 ± 1.7	0.96	0.17	0.07	30.6 ± 2.4
CeO_2	63.6 ± 2.1	6.0 ± 0.1	3.3 ± 0.2	27.1 ± 2.1	1.13	0.32	0.04	26.5 ± 3.0
ZrO_2	75.1 ± 4.5	6.5 ± 0.2	5.4 ± 0.4	13.0 ± 4.5	1.03	0.13	0.06	32.8 ± 6.4
$CeZrO_x$	74.4 ± 2.3	6.7 ± 0.2	4.7 ± 0.1	14.2 ± 2.4	1.08	0.14	0.05	32.7 ± 3.3
Ni/CeO_2	55.4 ± 3.6	6.6 ± 0.6	1.6 ± 0.3	36.4 ± 3.7	1.42	0.49	0.02	23.2 ± 5.2
Ni/ZrO_2	60.3 ± 1.6	7.0 ± 0.3	4.3 ± 0.6	28.4 ± 1.7	1.39	0.35	0.06	26.5 ± 2.4
$Ni/CeZrO_x$	70.5 ± 1.7	8.2 ± 0.4	4.2 ± 0.1	17.1 ± 1.7	1.40	0.18	0.05	32.7 ± 2.4

[a] By difference. [b] Calculated using the Dulong formula developed by Demirbas.[14] Ranges represent the standard deviation of either two or three repeated tests.

Table S5. The chemical oxygen demand (COD) and total organic carbon (TOC) of previous aqueous phase (AP) produced from HTL and CHTL of 15 wt% food waste at 300 °C and 60 min (unpublished data).

	TOC (mg L^{-1})	COD (mg L^{-1})

AP from HTL of WPI Food Waste[a]	14690	47070
AP from CHTL of WPI Food Waste[a]	16460	49465
AP from HTL of U Conn Food Waste[b]	17430	54733
AP from CHTL of U Conn Food Waste[b]	21300	58043

[a] The food waste was prepared at Worcester Polytechnic Institute. [b] the food waste was prepared in University of Connecticut.

The chemical oxygen demand of the aqueous phase is highly correlated to the corresponding TOC values (with R^2=0.89) based on the experimental data measured for our representative aqueous samples produced from previous CHTL of food waste under similar conditions (**Table S5**).

Table S6. Organic compounds distribution in bio-crude oils using different catalysts, characterized by GC-MS.

Chemical Groups	**Relative Peak Area (%)**							
	HTL (N_2)	**HTL (H_2)**	**CeO_2**	**ZrO_2**	**$CeZrO_x$**	**Ni/CeO_2**	**Ni/ZrO_2**	**Ni/$CeZrO_x$**
Fatty Acid Amides	69.2	73.7	77.7	60.4	73.7	56.9	65.0	72.0
Fatty Acid Esters	5.7	6.9	2.9	13.7	2.6	2.6	16.9	3.8
Cyclic & acyclic amides[a]	7.8	11.6	11.0	6.6	4.0	16.4	10.0	11.5
N-cyclic compounds[b]	4.2	-[d]	3.9	7.4	9.8	11.5	-[d]	2.4
O-cyclic compounds[c]	4.2	-[d]	-[d]	4.2	3.4	4.5	-[d]	-[d]
Ketones & Alcohols	8.9	7.9	3.1	6.0	4.8	8.1	8.0	10.2
Hydrocarbons	-[d]	-[d]	1.5	1.8	1.7	-[d]	-[d]	-[d]

[a] Excluding fatty acid amides. [b] Contains quinolines, pyridines, pyrroles, indolizines, indoles, pyridinols, etc. [c] Contains phenols. [d] below detection limit.

Table S7. Peak area ratios of protons adjacent to heteroatoms to methylene protons in different biocrude oil samples, obtained using ^{1}H NMR analysis.

Biocrude oil obtained using different catalysts	Peak area ratios of 2.09–2.18 ppm (protons adjacent to heteroatoms) to 1.18–1.26 ppm (methylene protons)
HTL(H_2)	0.53
CeO_2	0.37
ZrO_2	0.03
$CeZrO_x$	0.29
Ni/CeO_2	0.62
Ni/ZrO_2	0.21
Ni/$CeZrO_x$	0.27

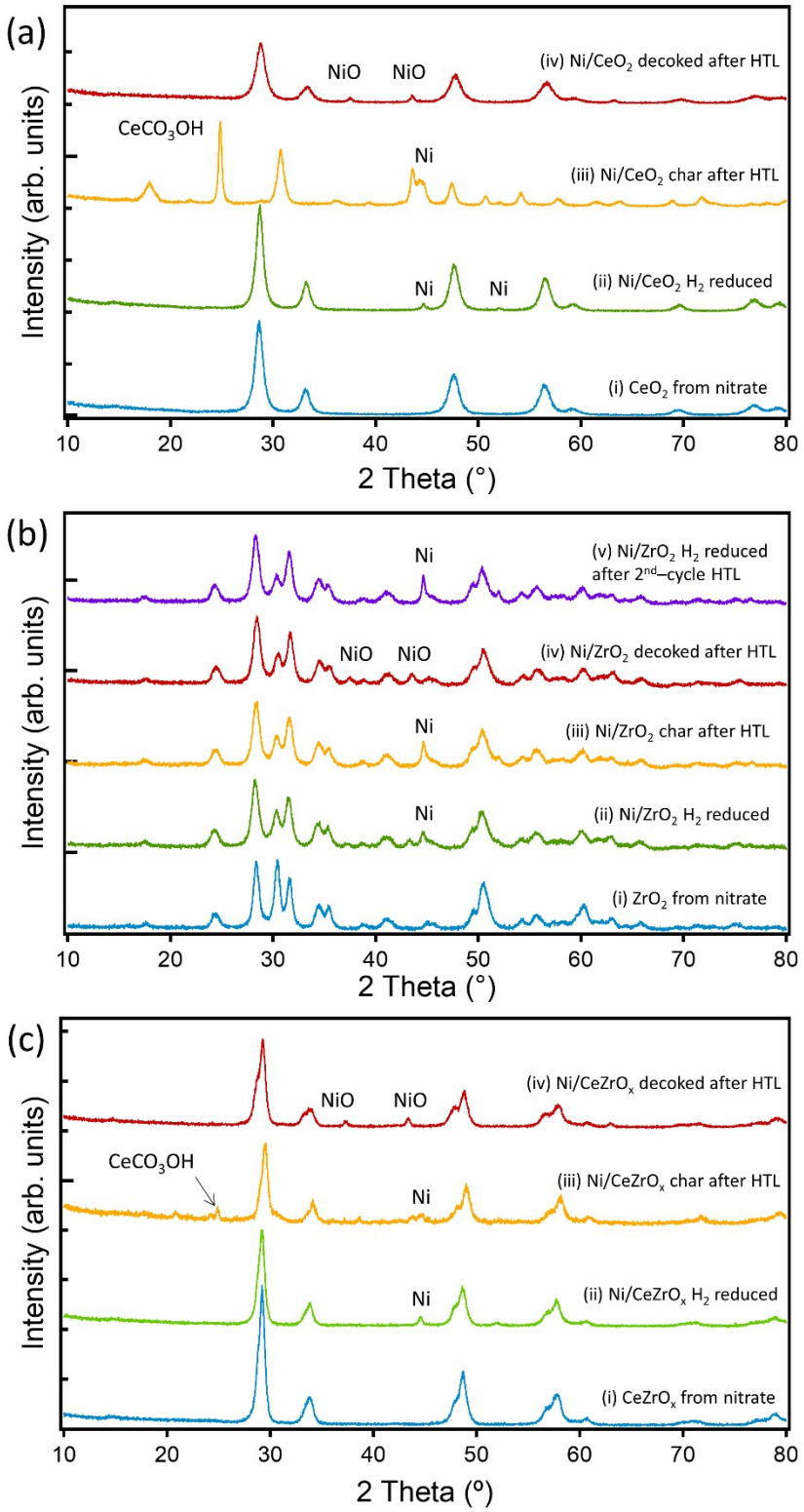

Figure S1. XRD patterns of metal oxides, reduced Ni impregnated metal oxides, used Ni impregnated metal oxides after HTL, and decoked Ni impregnated metal oxides after HTL for (a) CeO_2, (b) ZrO_2, and (c) $CeZrO_x$.

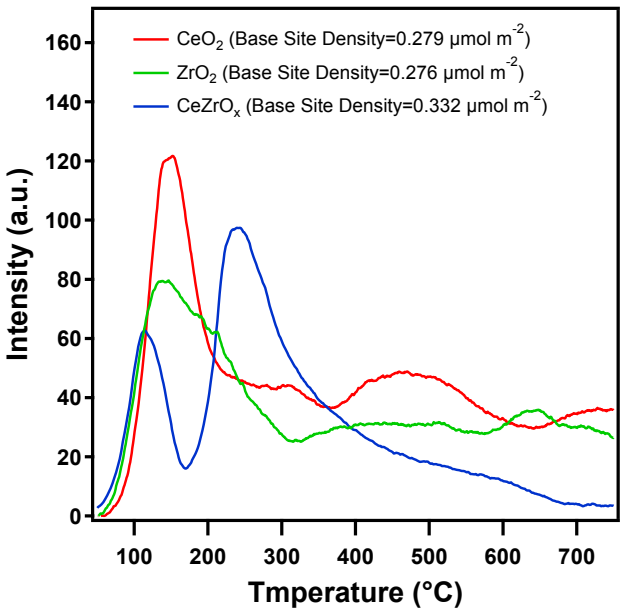

Figure S2. CO_2-TPD base site characterization of metal oxide catalysts.

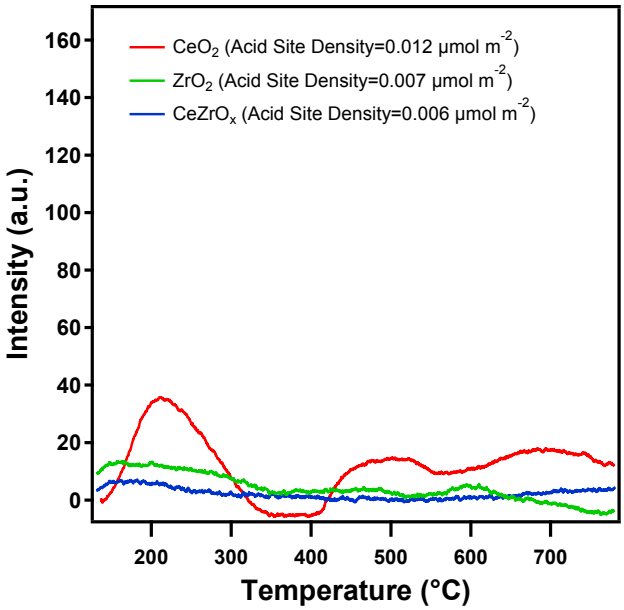

Figure S3. NH_3-TPD acid site characterization of metal oxide catalysts.

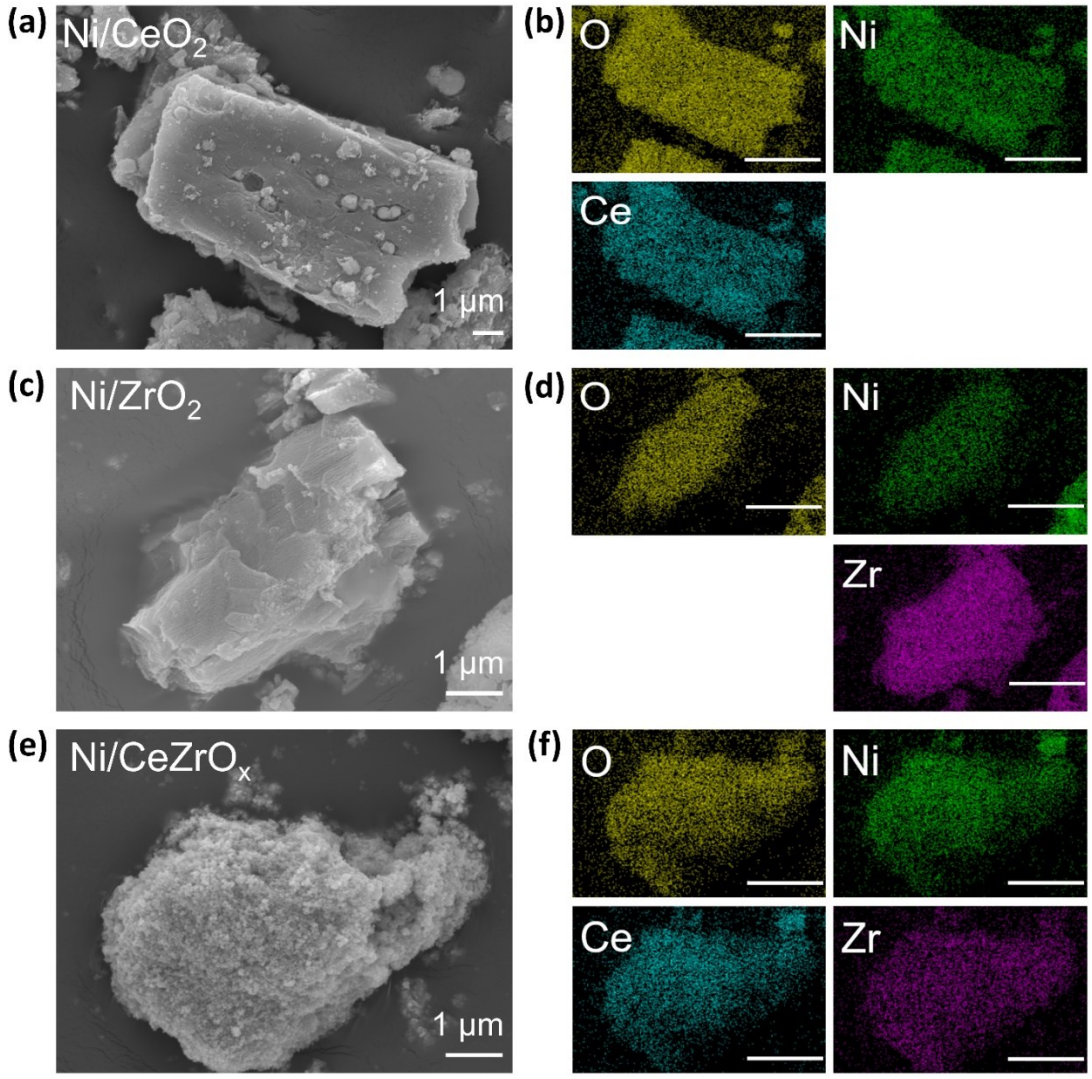

Figure S4. SEM images of (a) Ni/CeO_2, and (c) Ni/ZrO_2 and (e) $Ni/CeZrO_x$, and SEM-EDS maps of oxygen (O), nickel (Ni), cerium (Ce) and zirconium (Zr) present in (b) Ni/CeO_2, and (d) Ni/ZrO_2, and (f) $Ni/CeZrO_x$. The white scale bars displayed in the figures of EDS maps represent 2.5 μm.

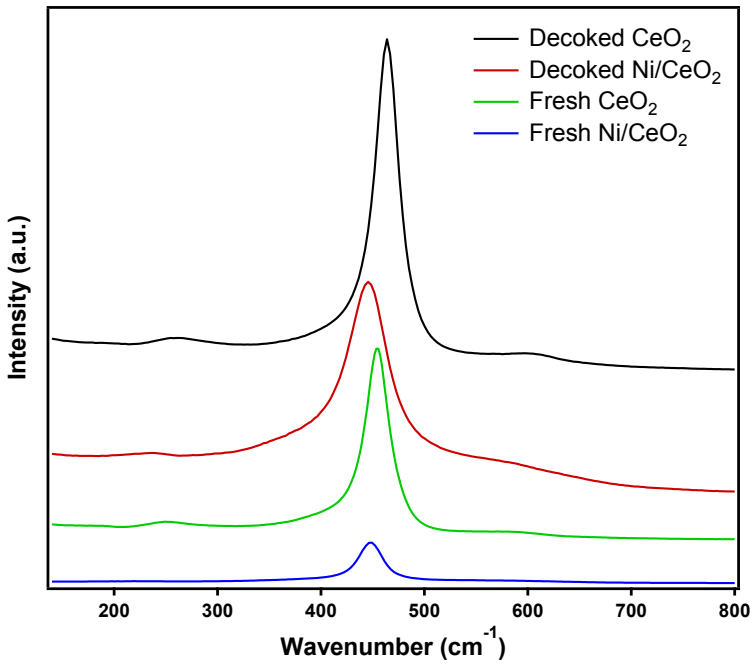

Figure S5. Raman spectra of fresh catalysts (CeO_2 and Ni/CeO_2) and the decoked catalysts (CeO_2 and Ni/CeO_2) generated from CHTL of 15 wt% food waste under 300 °C and 60 min.

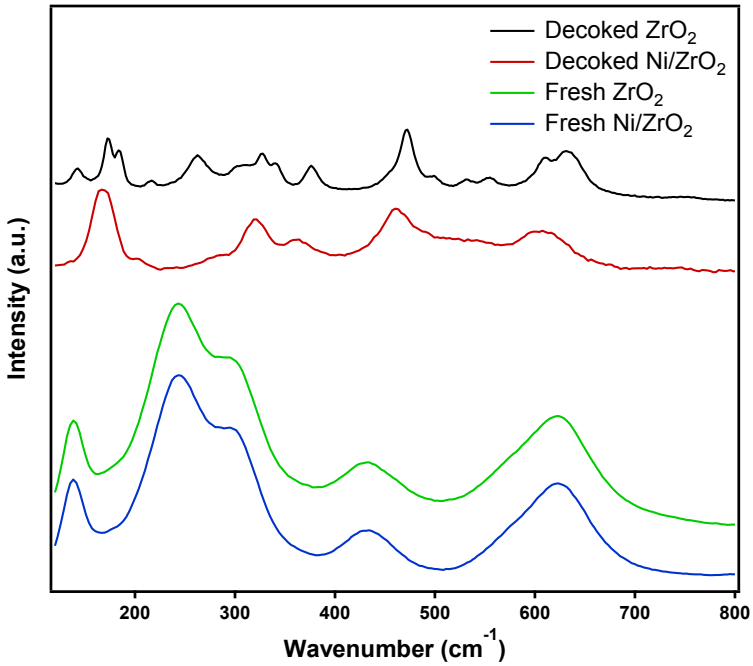

Figure S6. Raman spectra of fresh catalysts (ZrO_2 and Ni/ZrO_2) and the decoked catalysts (ZrO_2 and Ni/ZrO_2) generated from CHTL of 15 wt% food waste under 300 °C and 60 min.

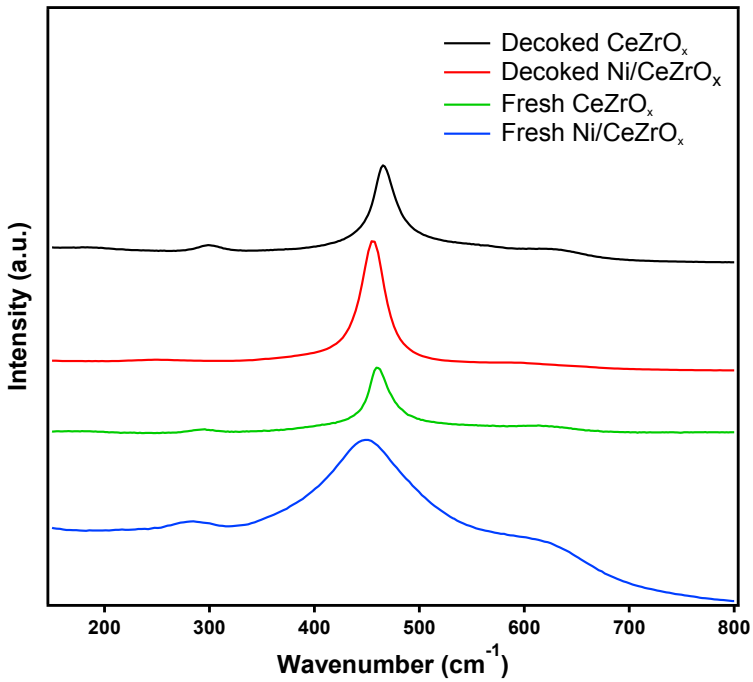

Figure S7. Raman spectra of fresh catalysts ($CeZrO_x$ and $Ni/CeZrO_x$) and the decoked catalysts ($CeZrO_x$ and $Ni/CeZrO_x$) generated from CHTL of 15 wt% food waste under 300 °C and 60 min.

Figure S5-S7 show that the F_{2g} peaks of cubic CeO_2 and Ni/CeO_2 at 453 cm^{-1}, the characteristic peaks of cubic ZrO_2 and Ni/ZrO_2 at 145, 246, 301, 436, and 625 cm^{-1}, and the broad peak containing the F_{2g} peak of cubic CeO_2 and the peak of tetragonal ZrO_2 existed in both $CeZrO_x$ and $Ni/CeZrO_x$ catalysts at 463-473 cm^{-1} were in good agreement with the corresponding results from previous studies.[15-17]

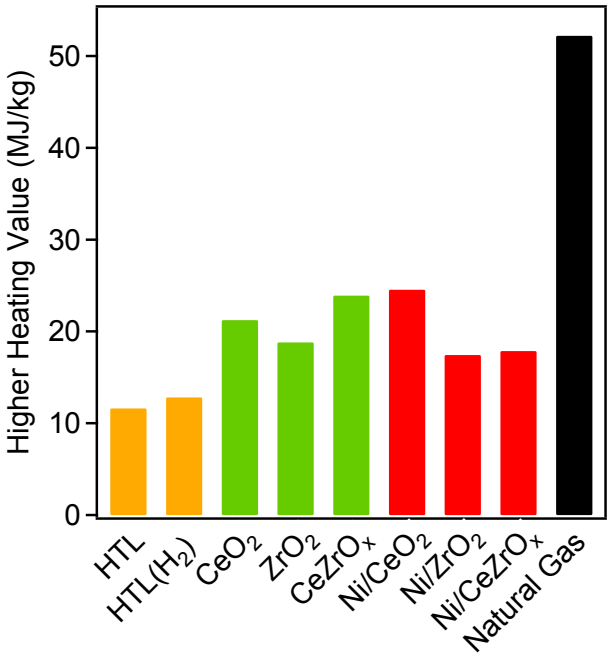

Figure S8. Estimated Higher heating values of gas produced from HTL of food waster without/with using transition metal oxide catalysts. The operating condition are 300 °C, 20.7 MPa for 60 min. Feed: Food waste, HTL: Thermal run (no H_2 or catalyst), HTL (H_2): Thermal run (with H_2 no catalyst).

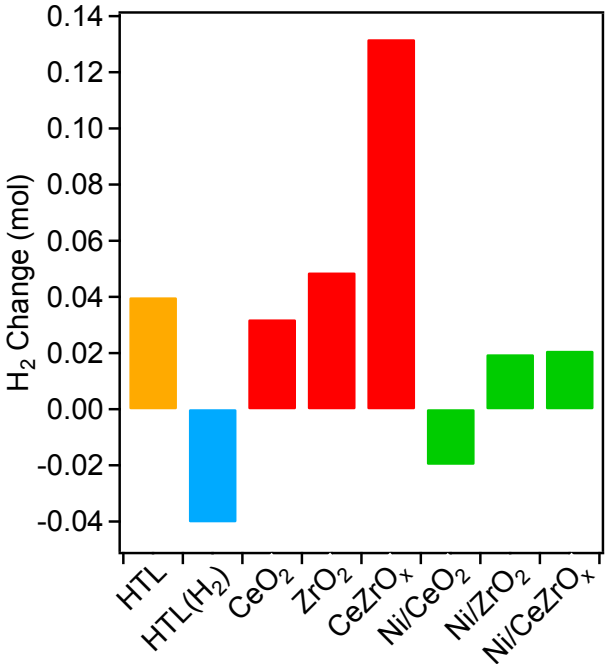

Figure S9. H_2 change between different HTL products with and without using H_2 and catalysts. The operating condition was 300 °C, ~20.7 MPa and 60 min.

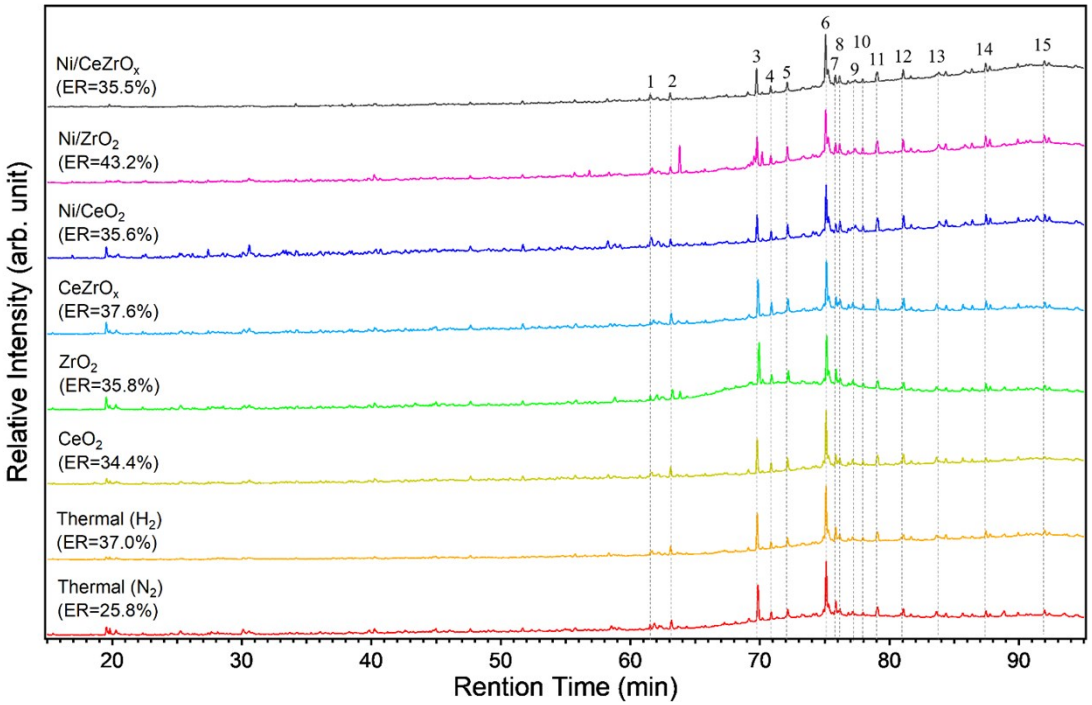

Figure S10. GC-MS chromatogram of the bio-crude oils produced using different catalysts under H_2 atmosphere. ER: Energy Recovery. (1) 61.7 min 3,6-bis(2-methylpropyl)piperazine-2,5-dione; (2) 63.1 min tetradecanamide; (3) 69.8 min tetradecanamide; (4) 70.9 min *N*-methyldodecanamide; (5) 72.1 min *N*,*N*-dimethyldodecanamide; (6) 75.1 min octadec-9-enamide, (Z)-; (7) 75.8 min octadecanamide; (8) 76.2 min *N*-butyloctadecanamide; (9) 77.4 min *N*,*N*-dimethyloctadec-9-enamide; (10) 77.9 min *N*,*N*-dimethyldodecanamide; (11) 79.1 min 1-morpholin-4-yldecan-1-one; (12) 81.1 min 1-pyrrolidin-1-yloctadecan-1-one; (13) 83.8 min (*E*)-*N*,*N*-bis(2-hydroxyethyl)octadec-9-enamide; (14) 87.4 min 10,13-dimethyl-17-(6-methylheptan-2-yl)-2,3,6,7,8,9,11,12,14,15,16,17-dodecahydro-1*H*-cyclopenta[a]phenanthrene; (15) 92.0 min (8*S*,9*S*,10*R*,13*R*,14*S*,17*R*)-10,13-dimethyl-17-[(2*R*)-6-methylheptan-2-yl]-2,3,4,7,8,9,11,12,14,15,16,17-dodecahydro-1*H*-cyclopenta[a]phenanthrene.

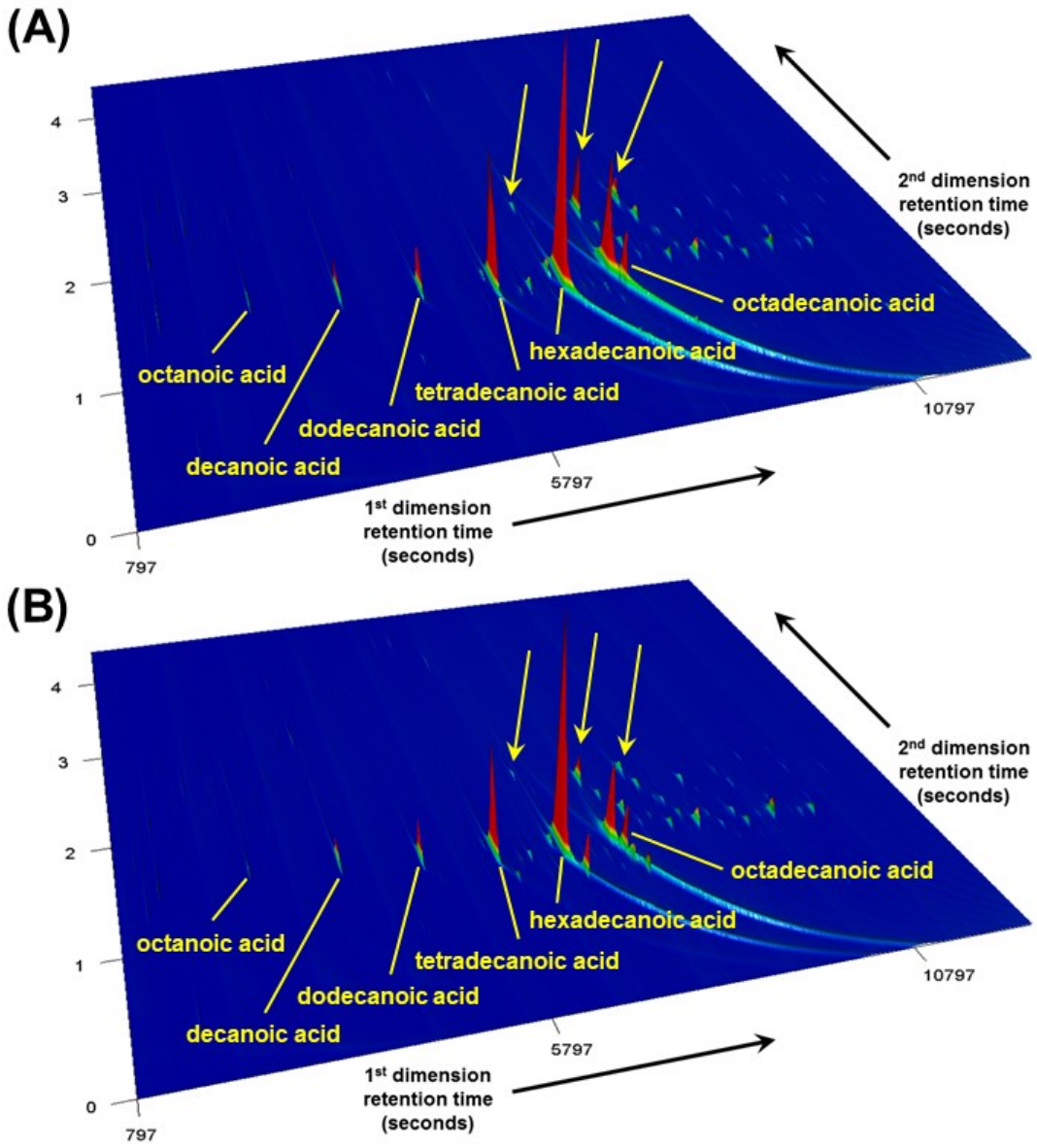

Figure S11. GC × GC−HRT selected ion mountain plot chromatograms of (A) bio-crude oil obtained from non-catalytic HTL reaction and (B) bio-crude oil obtained using Ni/ZrO_2 catalyst. Both chromatograms are scaled identically, and without sample derivatization. Yellow arrows represent C14–C18 fatty acid amides.

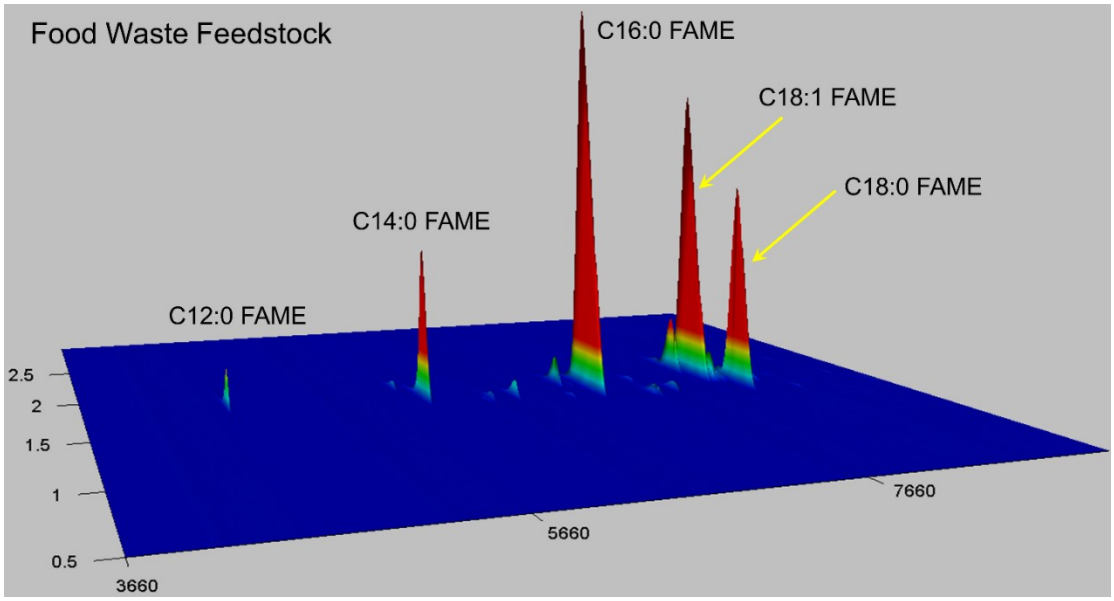

Figure S12. GC × GC FID chromatograms of fatty acid methyl esters distribution from food waste feedstock.

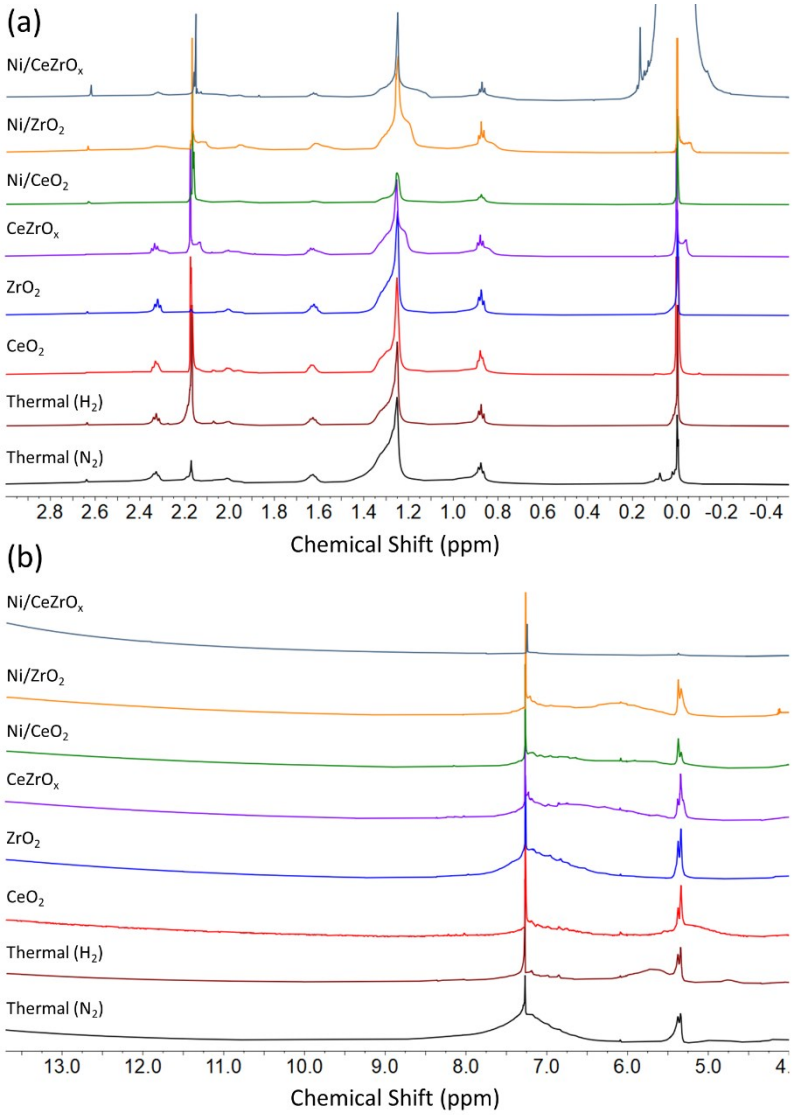

Figure S13. ^{1}H NMR spectra in bio-crude oils from 15 wt.% of food waste under 300 °C and 60 min with chemical shift of (a) 0–3 ppm and (b) 4–13ppm.

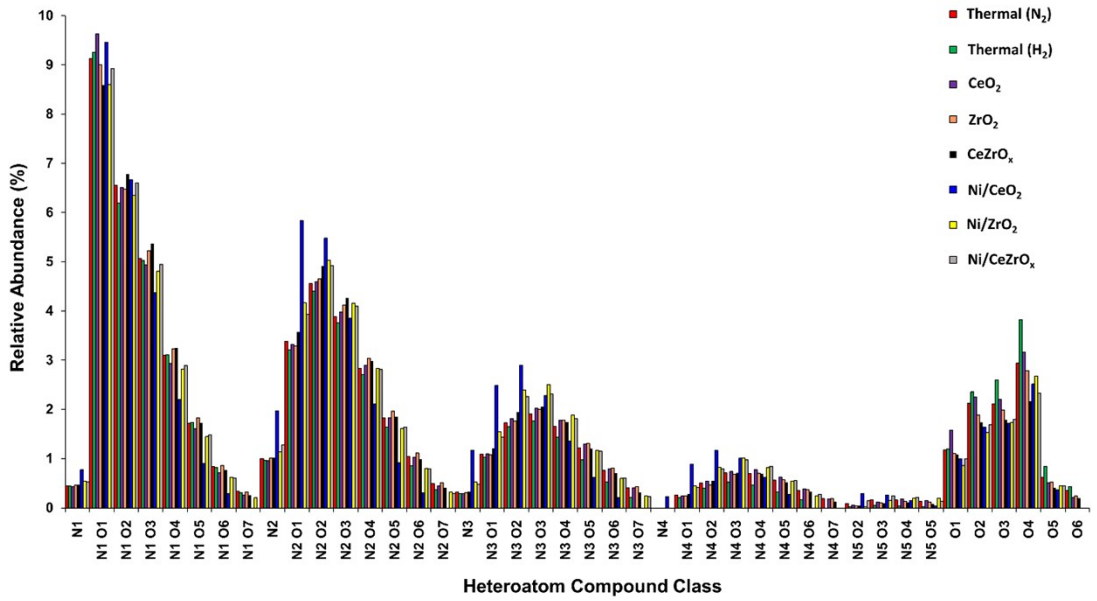

Figure S14. Heteroatom class distributions of bio-crude oil from CHTL of 15 wt% food waste under 300 °C and 60 min derived from positive-ion APPI FT-ICR MS.

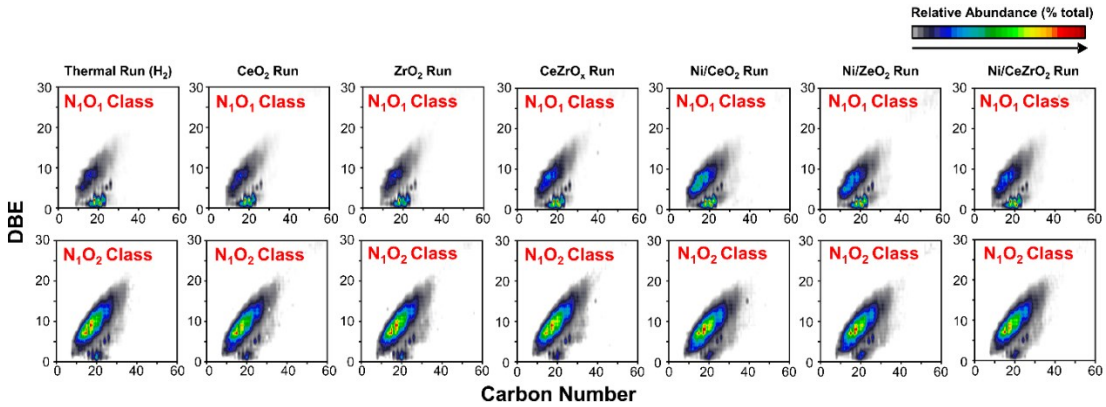

Figure S15. Color-coded isoabundance–contoured plots of DBE (double bond equivalents) versus carbon number for heteroatom N_1O_1 and N_1O_2 classes in bio-crude oils from 15 wt% of food waste under 300 °C and 60 min derived from positive-ion APPI FT-ICR MS.

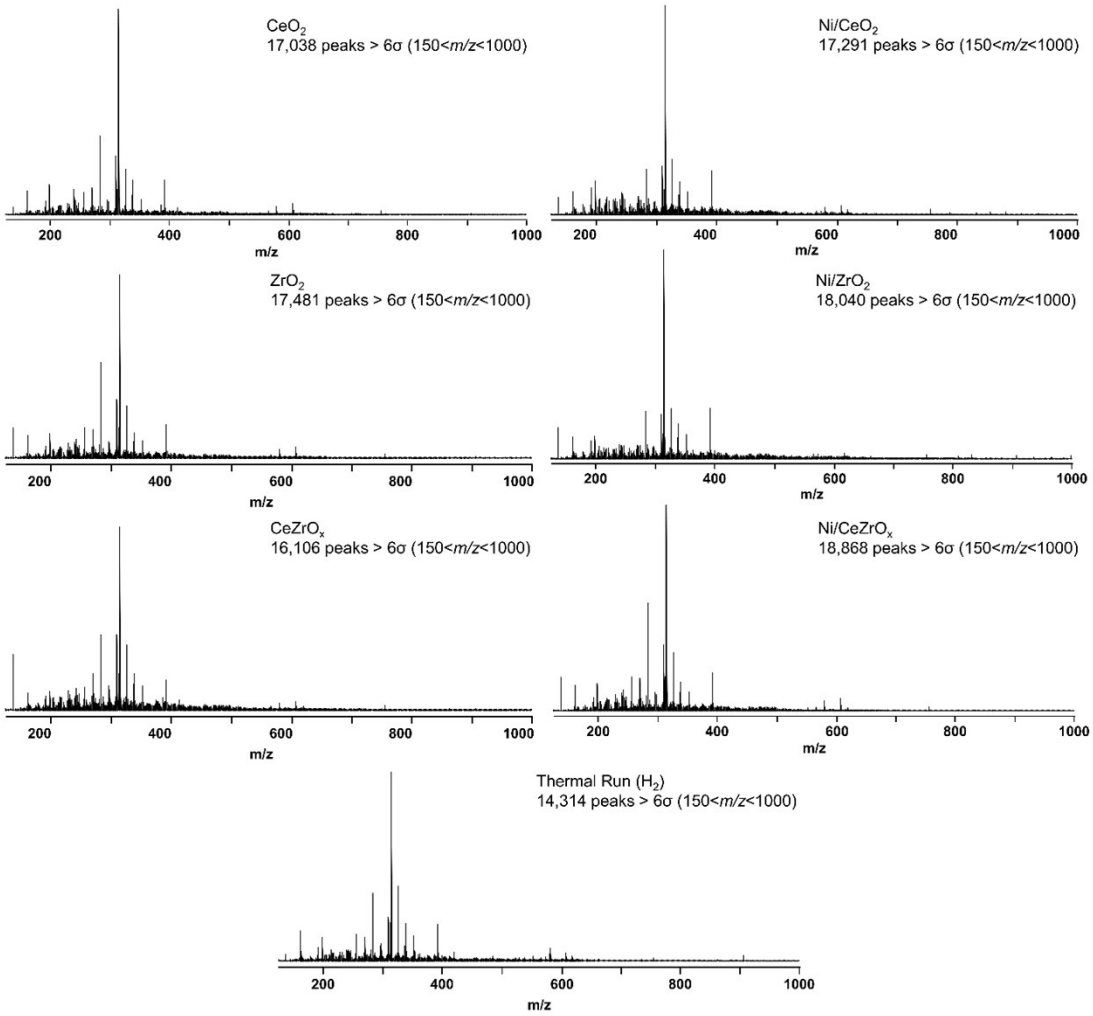

Figure S16. Positive-ion APPI FT-ICR MS broadband spectra of the bio-crude oil obtained under different conditions.

References

1. R. K. Nelson, K. M. Gosselin, D. J. Hollander, S. A. Murawski, A. Gracia, C. M. Reddy and J. R. Radović, *Energy & Fuels*, 2019, **33**, 3925-3933.

2. J. M. Purcell, C. L. Hendrickson, R. P. Rodgers and A. G. Marshall, *Analytical Chemistry*, 2006, **78**, 5906-5912.

3. N. K. Kaiser, J. P. Quinn, G. T. Blakney, C. L. Hendrickson and A. G. Marshall, *J. Am. Soc. Mass Spectrom.*, 2011, **22**, 1343-1351.

4. N. K. Kaiser, J. J. Savory and C. L. Hendrickson, *J. Am. Soc. Mass Spectrom.*, 2014, **25**, 943-949.

5. N. K. Kaiser, A. M. McKenna, J. J. Savory, C. L. Hendrickson and A. G. Marshall, *Anal. Chem.*, 2013, **85**, 265-272.

6. T. Chen, S. C. Beu, N. K. Kaiser and C. L. Hendrickson, *Rev. Sci. Instrum.*, 2014, **85**, 0666107/0666101-0066107/0666103.

7. I. A. Boldin and E. N. Nikolaev, *Rapid Commun. Mass Spectrom.*, 2011, **25**, 122-126.

8. G. T. Blakney, C. L. Hendrickson and A. G. Marshall, *Int. J. Mass Spectrom.*, 2011, **306**, 246-252.

9. J. J. Savory, N. K. Kaiser, A. M. McKenna, F. Xian, G. T. Blakney, R. P. Rodgers, C. L. Hendrickson and A. G. Marshall, *Anal. Chem.*, 2011, **83**, 1732-1736.

10. E. Kendrick, *Anal. Chem.*, 1963, **35**, 2146-2154.

11. C. A. Hughey, C. L. Hendrickson, R. P. Rodgers, A. G. Marshall and K. Qian, *Anal. Chem.*, 2001, **73**, 4676-4681.

12. F. W. McLafferty and F. Turecek, *Interpretation of Mass Spectra, 4th Ed.*, University Science Books, Mill Valley, CA, 1993.

13. Y. E. Corilo, *Petroorg Software*, Florida State University, Omics LLC, Tallahassee, Fl, 2014.

14. A. Demirbaş, *Fuel*, 1997, **76**, 431-434.

15. F. Liang, Y. Yu, W. Zhou, X. Xu and Z. Zhu, *Journal of Materials Chemistry A*, 2015, **3**, 634-640.

16. H. Xu, M. Sun, S. Liu, Y. Li, J. Wang and Y. Chen, *RSC advances*, 2017, **7**, 24177-24187.

17. S. N. Basahel, T. T. Ali, M. Mokhtar and K. Narasimharao, *Nanoscale research letters*, 2015, **10**, 73.